

# UCLA

## UCLA Previously Published Works

### Title

Mechanism and Dynamics of Intramolecular C-H Insertion Reactions of 1-Aza-2-azoniaallene Salts

### Permalink

<https://escholarship.org/uc/item/7nb0g83d>

### Journal

Journal of the American Chemical Society, 137(28)

### ISSN

0002-7863

### Authors

Hong, Xin  
Bercovici, Daniel A  
Yang, Zhongyue  
[et al.](#)

### Publication Date

2015-07-22

### DOI

10.1021/jacs.5b04474

Peer reviewed



Published in final edited form as:

*J Am Chem Soc.* 2015 July 22; 137(28): 9100–9107. doi:10.1021/jacs.5b04474.

## Mechanism and Dynamics of Intramolecular C-H Insertion Reactions of 1-Aza-2-azoniaallene Salts

Xin Hong<sup>‡,||</sup>, Dan Bercovici<sup>†,||</sup>, Zhongyue Yang<sup>‡</sup>, Nezar Al-Bataineh<sup>†</sup>, Ramya Srinivasan<sup>†</sup>, Ram C. Dhakal<sup>†</sup>, K. N. Houk<sup>‡</sup>, Matthias Brewer<sup>†</sup>

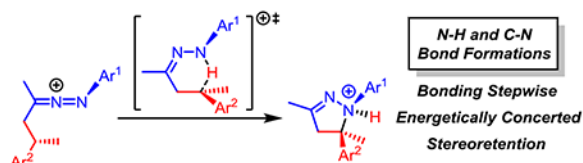
<sup>†</sup>Department of Chemistry, The University of Vermont, Burlington, Vermont 05405, United States

<sup>‡</sup>Department of Chemistry and Biochemistry, University of California, Los Angeles, California 90095, United States

### Abstract

The 1-aza-2-azoniaallene salts, generated from  $\alpha$ -chloroazo compounds by treatment with halophilic Lewis acids, undergo intramolecular C–H amination reactions to form pyrazolines in good to excellent yields. This intramolecular amination occurs readily at both benzylic and tertiary aliphatic positions and proceeds at an enantioenriched chiral center with retention of stereochemistry. Competition experiments show that insertion occurs more readily at an electron-rich benzylic position than an electron-deficient one. The C-H amination reaction only occurs with certain tethers connecting the heteroallene cation and the pendant aryl groups. With a longer tether or when the reaction is intermolecular, electrophilic aromatic substitution occurs instead of C-H amination. The mechanism and origins of stereospecificity and chemoselectivity were explored with density functional theory (B3LYP and M06-2X). The 1-aza-2-azoniaallene cation undergoes C-H amination through a hydride transfer transition state to form the N-H bond, and the subsequent C-N bond formation occurs spontaneously to generate the heterocyclic product. This concerted two-stage mechanism was shown by IRC and quasiclassical molecular dynamics trajectory studies.

### Graphical Abstract



**Corresponding Author:** houk@chem.ucla.edu; matthias.brewer@uvm.edu.

<sup>||</sup>X. H. and D. B. contributed equally.

### Supporting Information.

Experimental procedures, and full characterization of the products and spectra. Coordinates, absolute electronic energies and free energies in solution of DFT-computed stationary points. This material is available free of charge via the Internet at <http://pubs.acs.org>.

The authors declare no competing financial interest

## Introduction

C-H insertions of nitrogen centered radicals,<sup>1</sup> nitrenes,<sup>2</sup> and most notably, transition metal nitrenoids,<sup>3</sup> are valuable synthetic reactions. Based on Breslow and Gellman's seminal work,<sup>4</sup> Che,<sup>5</sup> Du Bois,<sup>6</sup> Driver,<sup>7</sup> Davies,<sup>8</sup> Lebel,<sup>9</sup> and Shi<sup>10</sup> have made C-H insertions of transition metal nitrenoids practical and stereoselective processes for natural product synthesis. Mechanistic studies indicate that both concerted and stepwise "radical rebound" processes can be operative in these transformations.<sup>11</sup>

The Brewer group has studied the reactivities of aryl 1-aza-2-azoniaallene salts in intramolecular reactions leading to nitrogen heterocycles.<sup>12</sup> These heteroallene species can be prepared directly from N-aryl hydrazones by oxidation or through the reaction of  $\alpha$ -chloroazo compounds with halophilic Lewis acids. As shown in Scheme 1, these species, which can also be considered as imino-nitrenium cations, undergo direct insertion into pendant benzylic C-H bonds to afford pyrazolines.<sup>12d</sup>

These 1-aza-2-azoniaallene salts are also known to react with pendant alkenes in (3+2) or [4+2] cycloadditions to provide various heterocycles, as shown in Scheme 2.<sup>12a-c,e</sup> The chemo- and regioselectivity of the cycloaddition reactions were found to be controlled by the length of the tether that connects the reacting components. We recently studied these cycloaddition reactions computationally to understand the origins of these substrate-dependent reactivities.<sup>13</sup> We have now studied the scope of the insertion reaction experimentally, and established the mechanism and determined the origins of selectivities in the insertion process through computation.

## Results and Discussion

### Experimental Results

Our initial report of the C-H insertion reactivity of aryl 1-aza-2-azoniaallene salts (Table 1), indicated that heteroallenes with electron-rich N-aryl groups provided higher yields of insertion products than those with electron-poor N-aryl groups (entry 1 vs 2, Table 1).<sup>12d</sup> The electronic properties of the pendant aryl group also affected the C-H insertion (entry 3-6, Table 1). Electron-rich methoxy derivatives gave notably higher yields of insertion, but there was little difference in yield between substrates with neutral and electron-deficient aryl rings (entries 4 and 5). A competition experiment showed that the insertion occurred more readily adjacent to an electron-rich aryl ring than an electron-deficient one (entry 6). No insertion was observed at a secondary aliphatic center, but insertion did occur at a tertiary aliphatic center. The reaction in Scheme 3 showed that insertion at a chiral tertiary benzylic position occurs with retention of stereochemical purity.

We have now obtained further experimental data that define the scope and the mechanism of this insertion reaction. We explored the effect of tether length on intramolecular C-H insertions. The  $\alpha$ -chloroazo **8a** was treated with Lewis acid, AlCl<sub>3</sub>, to generate the corresponding 1-aza-2-azoniaallene salt. This heteroallene, which has a tether that is one methylene unit longer than the tether in **1a**, does not undergo the C-H insertion, but instead reacts with the pendant aryl group in an electrophilic aromatic substitution reaction to give

azotetralin **9a** in 76% yield (Scheme 4). This reactivity highlights the electrophilic nature of heteroallene salts, and shows that tether length plays an important role in determining the result of these reactions. This Friedel-Crafts-type reactivity is not limited to intramolecular reactions; the heteroallene derived from acetone reacted with toluene to give azo-cymene **9b** in 30% yield (Scheme 4).

Unlike the well-established allylic C-H aminations with transition metal catalysts, the linear 1-aza-2-azoniaallene salts, such as **4a** and **6a**, undergo [4+2] or 1,3-monopolar<sup>14</sup> cycloadditions with pendant alkenes (Scheme 2). In order to achieve the allylic C-H amination, we prepared a heteroallene salt of cyclopentene derivative **1i**, which would undergo [4+2] cycloaddition only with difficulty due to conformational constraints. Indeed, this substrate underwent allylic insertion instead of cycloaddition to give pyrazoline **3i** in 69% yield (Scheme 5).

We also studied competition between C-H insertion at benzylic and tertiary aliphatic positions. As a point of comparison, previous studies show that rhodium nitrenoids insert more readily at tertiary aliphatic centers than benzylic positions,<sup>15</sup> whereas ruthenium<sup>6h</sup> and iron<sup>16</sup> based catalysts select for benzylic or allylic positions, and the selectivity of silver catalysts is ligand dependent.<sup>17</sup> To assess the chemoselectivity of 1-aza-2-azoniaallene salt insertions, we prepared the heteroallene salt derived from 5-methyl-1-phenylhexan-3-one (**1j**); insertion occurred almost exclusively at the benzylic position (Scheme 6).

We also conducted a kinetic isotope effect (KIE) study using an internal competition experiment. The requisite deuterium enriched ketone precursor of  $\alpha$ -chloroazo **1k** was prepared by the conjugate reduction procedure described by Keinan and Greenspoon.<sup>18</sup> Subjecting **1k** to the C-H amination reaction conditions provided an average 4.3 : 1 ratio of deuterated to non-deuterated insertion products (**3k** and **3k'**), as determined by <sup>1</sup>H NMR integration of duplicate experiments (Scheme 7). Changing the N-aryl ring to p-tolyl had no effect on the selectivity. KIE studies have been widely applied in mechanistic investigations of other C-H amination reactions. Typically, aminations that occur by a radical rebound mechanism have high KIEs (in the range of 6-12),<sup>5a</sup> since the transition state involves mainly hydrogen atom transfer. By contrast, aminations that proceed through concerted insertion mechanisms show significantly lower KIEs (typically 1-3).<sup>15,6h</sup> KIEs between 3 and 6 seem to indicate rapid radical rebound mechanisms<sup>17,19</sup> or highly asynchronous concerted insertions.<sup>6h,9c,20,21</sup> The relatively high primary isotope effect of 4.3 suggests the latter mechanism.

## Computational Methods

DFT calculations were performed with Gaussian 09.<sup>22</sup> Geometry optimizations were carried out with B3LYP functional and the 6-31G(d) basis set. The vibrational frequencies were computed at the same level to check whether each optimized structure is an energy minimum or a transition state and to evaluate its zero-point vibrational energy (ZPVE) and thermal energies at 298 K. Single-point energies were computed with the M06-2X functional<sup>23</sup> and the 6-311+G(d,p) basis set. Solvation energy corrections for dichloromethane were evaluated by a self-consistent reaction field (SCRF) using the SMD<sup>24</sup>

model under the same level of theory as the single point energy calculation (M06-2X/6-311+(d,p)).

The reaction mechanism and timing of bond formations were studied by quasiclassical trajectories at 298 K, with B3LYP and the 6-31G\* basis set. All dynamics calculations were performed with Progdyn<sup>25</sup>, with which the classical equations of motion are integrated with Velocity Verlet algorithm. Energies and derivatives were computed “on the fly” using Gaussian 09 with a 1 fs integration step-size. Trajectories were initialized, from the structure of the transition state TS11, by TS normal mode sampling, and were then propagated in both reactants and products directions.<sup>26</sup>

## Computational Results

**Reaction Mechanism**—We first studied the insertion reaction mechanism for the 1-aza-2-azoniaallene cation **10** (Figure 1). The optimized structures of transition states and the free energy changes on the singlet and triplet pathways are shown in Figure 1. From the singlet species **10**, C-H amination can occur through transition state **TS11**, with a free energy barrier of 20.0 kcal/mol, leading to the protonated heterocyclic product **12**.

Azoniaallene **10** has two moieties that can react, the cationic heterocumulene part and the pendant benzylic C-H bond. In the singlet transition state **TS11**, the major orbital interaction between the reacting fragments occurs between the LUMO of the 1,3-monopolar heterocumulene fragment and the HOMO of the benzylic C-H bond. This suggests that a hydride abstraction occurs initially to the electron deficient heterocumulene, forming a N-H bond and a benzyl carbocation. This benzyl carbocation then forms a C-N bond with the remaining lone pair on nitrogen to give the insertion product.

Alternatively, **10** could undergo a spin transition to generate the triplet diradical species, **13**, which could react through a triplet C-H amination pathway.<sup>27</sup> However, the triplet **13** is 23.9 kcal/mol less stable than **10**, making the triplet pathway much less favorable as compared with the singlet pathway.

**Origins of Stereospecificity of the Singlet C-H Amination Pathway**—The bonding stepwise process of the C-H amination seems at odds with the stereoselectivity observed for insertion at a chiral benzylic position (Scheme 3). The origins for the stereospecificity is, however, explained by the intrinsic reaction coordinate (IRC) of **TS11**, shown in Figure 2. Starting from the substrate (point 1), the benzylic hydride gradually moves to the electron deficient terminal nitrogen via the transition state (point 21) to form the N-H bond (points 1 through 23). At point 23, the N-H bond is fully formed with a distance of 1.02 Å, but the C-N distance is still 2.54 Å. The subsequent C-N bond formation then occurs spontaneously, leading to the heterocyclic product (points 23 through 37). This IRC trajectory indicates that while the singlet C-H amination process is bonding stepwise, it is energetically concerted. That is, from substrate to product there is only one saddle point and, after the hydride transfer, there is no stable intermediate; the two consecutive bond formations are energetically concerted and occur via one transition state. This is a “nitrogen rebound”, in analogy to the “oxygen rebound”, which is well-known for cytochrome P-450<sup>28</sup> and other related oxidations, like that of dioxirane<sup>29</sup>.

In order for the insertion to occur at a chiral center without stereomutation, C-N bond formation must occur much faster than C-C bond rotation that would erode the stereoselectivity, by allowing bond formation with inversion of configuration. To test whether the proposed mechanism accounts for the experimentally observed stereoselectivity, we also studied the insertion pathway through quasiclassical molecular dynamics trajectories to provide information about the timing of bond formations. Quasiclassical trajectories were initialized by transition-state normal mode sampling with the Progdyn program developed by Singleton.<sup>25</sup> An ensemble of transition states was sampled based on Boltzmann distributions. These form a dividing surface intersecting the saddle point on the potential energy surface. The overlay of sampled transition state geometries and the corresponding C-N and N-H bond length distributions are shown in Figure 3. Both C-N and N-H bond lengths are distributed symmetrically with respect to the bond lengths of the saddle point (marked with green lines in Figure 3). This distribution of bond length is Gaussian, and we define the transition zone as the 98% confidence interval of the Gaussian distribution. The transition zones for the C-N bond and the N-H bond are  $2.48 \pm 0.12 \text{ \AA}$  and  $1.30 \pm 0.10 \text{ \AA}$  respectively. This means that 98% of the C-N and N-H bond lengths sampled are within  $\pm 0.12 \text{ \AA}$  and  $\pm 0.10 \text{ \AA}$  of the respective bond lengths at the saddle point.

Sampled transition states were propagated forwards and backwards by Newtonian equations of motion until they reached reactants or products. The fully formed bond length is defined as  $1.10 \text{ \AA}$  for N-H and  $1.80 \text{ \AA}$  for C-N. The corresponding reactant distances for reactant are  $3.00 \text{ \AA}$  for both bonds. Trajectories were terminated after 500 fs if they had not reached reactant or product in that period. A total of 256 trajectories was computed, and 95% of these were productive. Figure 4(a) illustrates one typical productive trajectory: starting from the substrate, the benzylic hydride moves to the terminal nitrogen until the N-H bond is about  $1.1 \text{ \AA}$ , but at this time point, the C-N distance is still around  $2.5 \text{ \AA}$ . The subsequent C-N bond formation occurs spontaneously, accompanied by some residual vibration of the just-formed C-H bond, with the formation of the heterocyclic product. Figure 4(b) shows two typical unproductive trajectories, which recross in the reactant or product side, and Figure 4(c) shows the overlay of all 256 trajectories.

Figure 5(a) shows the distribution of timing of bond formations for all productive trajectories. Starting from the sampled transition state starting geometries, the median time for N-H bond formation (reaching  $1.10 \text{ \AA}$ ) is 8 fs, and the median time for C-N bond formation (reaching  $1.80 \text{ \AA}$ ) is 75 fs; the timing of C-N bond formation is on average 67 fs later than that of N-H bond formation, essentially within a C-N vibrational period. This indicates that the N-H bond forms almost immediately after the transition state saddle point, which is in line with the IRC calculations (Figure 2), and that the C-N bond forms spontaneously afterwards within a short period of time. We also calculated the time gap between the formation of the C-N and N-H bonds for each productive trajectory. The distribution of time gaps is shown in Figure 5(b). The time gap of bond formation only ranges from 35 fs to 130 fs with the median located at 66 fs. This indicates a short time window between bond formation. Because the time scale of C-C bond rotation is generally higher than 1 ps, there is insufficient time for a C-C bond rotation to occur between the N-H and C-H bond forming events.

**Substituent Effect on the Reactivity of C-H Amination**—We have also studied the reaction barriers for substrates with a variety of substitutions on the  $\beta$ -phenyl ( $R^1$ ) or in place of this group, results are shown in Table 2. The  $\alpha$ -methylene of  $R^1$  in the substituted 1-aza-2-azoniaallene salt is a hydride donor, and substituents that stabilize the forming carbocation increase the C-H amination reactivities. Replacing the phenyl group (entry 1) by hydrogen (entry 2) increases the barrier dramatically from 20.0 kcal/mol with phenyl to 31.4 kcal/mol with hydrogen. Substitution by alkyl groups (entries 3 to 6) does not stabilize the forming carbocation as much as the phenyl group, and the reaction barrier increases to 21–23 kcal/mol. The electronic effect has a strong effect on the barrier. The reaction barrier increases significantly with electron-withdrawing substituents (entries 7 to 11), while electron-donating groups reduce the barrier dramatically (entries 12 and 13). Various electron-rich vinyl and aryl substituents have achievable amination barriers (entries 14, 16, 20–22). The energy barriers computed for the *p*-NO<sub>2</sub>-Ph and *p*-MeO-Ph derivatives (entries 19 and 22) are consistent with the selectivity observed in the competition experiment (Table 1, entry 6). We also computed amination at a tertiary C-H using the 1-aza-2-azoniaallene cation generated from substrate **1j** as a model, and the barrier is 17.2 kcal/mol.<sup>30</sup> The additional alkyl substituent lowers the barrier of amination by stabilizing the forming carbon cation in the transition state, making it competitive with benzylic C-H amination.

**Tether Effect on the Competition between C-H Amination and Electrophilic Aromatic Substitution**—We also explored the tether effect on the competition between the C-H amination and electrophilic aromatic substitution (Table 3). When there is one methylene between the heteroallene component and the benzylic hydride donor ( $n = 1$ ), the C-H amination transition state is 1.3 kcal/mol more stable than the electrophilic aromatic substitution transition state, because of the proximity of the reacting partners in **TS16** and the strain in **TS17**. This preference is also in line with the experimental results that this tether causes the C-H amination. With longer tethers ( $n = 2, 3$ ), the chemoselectivity is reversed, and the aromatic substitution is significantly more favorable than C-H amination.<sup>31</sup> A similar preference is also found in intermolecular reactions; the C-H amination between the corresponding 1-aza-2-azoniaallene and toluene has a barrier of 34.4 kcal/mol, while the barrier of electrophilic aromatic substitution is only 26.5 kcal/mol. Therefore, the electrophilic aromatic substitution is intrinsically much more favorable than the C-H amination. Only with the short tether ( $n = 1$ ), the ring strain of the two competing transition states significantly favors the C-H amination, leading to the reversed chemoselectivity.

## Conclusions

The scope, mechanism and dynamics of C-H amination reactions of 1-aza-2-azoniaallene salts have been studied experimentally and computationally. The facility of this C-H amination relies heavily on the tether that connects the heteroallene cation component and the pendant aryl groups. While the insertion occurs readily at benzylic and tertiary aliphatic positions when the tether is two methylene units, a longer tether or intermolecular reaction gives electrophilic aromatic substitution, the intrinsically favored reaction, rather than C-H amination.

This C-H amination proceeds through a hydride transfer transition state to form a N-H bond initially, and the subsequent C-N bond formation occurs spontaneously afterwards to generate the heterocyclic product. IRC trajectory indicates that the two consecutive bond formation processes, N-H and C-N, are energetically concerted, and this concerted mechanism is further proved by quasiclassical molecular dynamics trajectory studies. The C-N bond formation occurs much faster than C-C bond rotation, which explains the stereospecificity in the C-H amination. In line with the hydride transfer transition state, electron-rich aryl substituents that stabilize the forming carbon cation facilitate the amination significantly, while alkyl and electron-poor aryl substituted substrates have higher reaction barriers.

## ACKNOWLEDGMENT

We are grateful to the National Scientific Foundation (CHE-1361104 to K.N.H. and CHE-1362286 to M.B.) for financial support of this research. Calculations were performed on the Hoffman2 Cluster at UCLA and the Extreme Science and Engineering Discovery Environment (XSEDE), which is supported by the NSF (OCI-1053575). Mass spectrometry data was acquired by Bruce O'Rourke on instruments purchased through instrumentation grants provided by the NSF (CHE-0342861) and the NIH (S10 OD018126).

## REFERENCES

- (1). For selected reviews, see:(a)Danen WC; Neugebauer FA *Angew. Chem., Int. Ed* 1975, 14, 783. (b)Stella L *Angew. Chem., Int. Ed* 1983, 22, 337.(c)Zard SZ *Chem. Soc. Rev* 2008, 37, 1603. [PubMed: 18648685] For recent examples, see:(d)Cecere G; König CM; Alleva JL; MacMillan DWC *J. Am. Chem. Soc* 2013, 135, 11521. [PubMed: 23869694] (e)Allen LJ; Cabrera PJ; Lee M; Sanford MS *J. Am. Chem. Soc* 2014, 136, 5607. [PubMed: 24702705] (f)Foo K; Sella E; Thomé I; Eastgate MD; Baran PS *J. Am. Chem. Soc* 2014, 136, 5279. [PubMed: 24654983] (g)Kim H; Kim T; Lee DG; Roh SW; Lee C *Chem. Commun* 2014, 50, 9273.(h)Qin Q; Yu S *Org. Lett* 2014, 16, 3504. [PubMed: 24964153] (i)Greulich TW; Daniliuc CG; Studer A *Org. Lett* 2015, 17, 254. [PubMed: 25541887] (j)Louillat-Habermeyer M-L; Jin R; Patureau FW *Angew. Chem., Int. Ed* 2015, 54, 4102.
- (2). For selected reviews, see:(a)Collet F; Lescot C; Liang C; Dauban P *Dalton Trans.* 2010, 39, 10401. [PubMed: 20931128] (b)Dequize G; Pons V; Dauban P *Angew. Chem., Int. Ed* 2012, 51, 7384.
- (3). For selected reviews, see:(a)Che C-M; Lo VK-Y; Zhou C-Y; Huang J-S *Chem. Soc. Rev* 2011, 40, 1950. [PubMed: 21387046] (b)Davies HML; Lian Y *Acc. Chem. Res* 2012, 45, 923. [PubMed: 22577963] (c)Yamaguchi J; Yamaguchi AD; Itami K *Angew. Chem., Int. Ed* 2012, 51, 8960.
- (4). (a)Breslow R; Gellman SL *J. Chem. Soc., Chem. Commun* 1982, 1400.(b)Breslow R; Gellman SL *J. Am. Chem. Soc* 1983, 105, 6728.
- (5). (a)Au S-M; Huang J-S; Yu W-Y; Fung W-H; Che C-M *J. Am. Chem. Soc* 1999, 121, 9120.(b)Yu X-Q; Huang J-S; Zhou X-G; Che C-M *Org. Lett* 2000, 2, 2233 [PubMed: 10930251] (c)Liang J-L; Yuan S-X; Huang J-L; Yu W-Y; Che C-M *Angew. Chem., Int. Ed* 2002, 41, 3465.(d)Leung SK-Y; Tsui W-M; Huang J-S; Che C-M; Liang J-L; Zhu N *J. Am. Chem. Soc* 2005, 127, 16629. [PubMed: 16305252] (e)Thu HY; Yu WY; Che C-M *J. Am. Chem. Soc* 2006, 128, 9048. [PubMed: 16834374] (f)Lin X; Zhao C; Che C-M; Ke Z; Phillips DL *Chem. Asian J* 2007, 2, 1101. [PubMed: 17712831] (g)Liu Y; Guan X; Wong EL-M; Liu P; Huang J-S; Che C-M *J. Am. Chem. Soc* 2013, 135, 7194. [PubMed: 23634746] (h)Wei J; Xiao W; Zhou C-Y; Che C-M *Chem. Commun* 2014, 50, 3373.(i)Liu Y; Chen G-Q; Tse C-W; Guan X; Xu Z-J; Huang J-S; Che C-M *Chem. Asian J* 2015, 10, 100. [PubMed: 25210011]
- (6). (a)Espino CG; Du Bois J *Angew. Chem., Int. Ed* 2001, 40, 598.(b)Hinman A; Du Bois J *J. Am. Chem. Soc* 2003, 125, 11510. [PubMed: 13129349] (c)Espino CG; Fiori KW; Kim M; DuBois J *J. Am. Chem. Soc* 2004, 126, 15378. [PubMed: 15563154] (d)Fleming JJ; Du Bois J *J. Am. Chem. Soc* 2006, 128, 3926. [PubMed: 16551097] (e)Kurokawa T; Mihyong K; Du Bois J *Angew. Chem., Int. Ed* 2009, 48, 2777.(f)Du Bois J *Org. Process Res. Dev* 2011, 15, 758.



- [PubMed: 21804756] (g)Olson DE; Maruniak A; Malhotra S; Trost BM; Du Bois J *Org. Lett* 2011, 13, 3336. [PubMed: 21618989] (h)Harvey ME; Musaev DG; Du Bois J *J. Am. Chem. Soc* 2011, 133, 17207. [PubMed: 21981699] (i)Roizen JL; Harvey ME; Du Bois J *Acc. Chem. Res* 2012, 45, 911. [PubMed: 22546004] (j)Olson DE; Roberts DA; Du Bois J *Org. Lett* 2012, 14, 6174. [PubMed: 23227976] (k)Roizen JL; Zalatan DN; Du Bois J *Angew. Chem., Int. Ed* 2013, 52, 11343. (l)Bess EN; Deluca RJ; Tindall DJ; Oderinde MS; Roizen JL; Du Bois J; Sigman MS *J. Am. Chem. Soc* 2014, 136, 5783. [PubMed: 24673332] (m)Olson DE; Su JY; Roberts DA; Du Bois J *J. Am. Chem. Soc* 2014, 136, 13506. [PubMed: 25233140]
- (7). (a)Stokes BJ; Dong H; Leslie BE; Pumphrey AL; Driver TG *J. Am. Chem. Soc* 2007, 129, 7500. (b)Shen M; Leslie BE; Driver TG *Angew. Chem., Int. Ed* 2008, 47, 5056. (c)Sun K; Sachwani R; Richert KJ; Driver TG *Org. Lett* 2009, 11, 3598. [PubMed: 19627144] (d)Nguyen Q; Sun K; Driver TG *J. Am. Chem. Soc* 2012, 134, 7262. [PubMed: 22519742] (e)Nguyen Q; Nguyen T; Driver TG *J. Am. Chem. Soc* 2013, 135, 620. [PubMed: 23265139] (f)Kong C; Jana N; Driver TG *Org. Lett* 2013, 5, 824.
- (8). (a)Reddy RP; Davies HML *Org. Lett* 2006, 8, 5013. [PubMed: 17048831] (b)Davies HML; Manning JR *Nature* 2008, 451, 417. [PubMed: 18216847] (c)Alford J; Davies HML *J. Am. Chem. Soc* 2014, 136, 10266. [PubMed: 24998910]
- (9). (a)Lebel H; Huard K; Lectard S *J. Am. Chem. Soc* 2005, 127, 14198. [PubMed: 16218610] (b)Lebel H; Huard K *Org. Lett* 2007, 9, 639. [PubMed: 17243710] (c)Huard K; Lebel H *Chem. Eur. J* 2008, 14, 6222. [PubMed: 18512829] (d)Lebel H; Spitz C; Leogane O; Trudel C; Parmentier M *Org. Lett* 2011, 13, 5460. [PubMed: 21919470] (e)Lebel H; Trudel C; Spitz C *Chem. Commun* 2012, 48, 7799. (f)Lebel H; Piras H; Bartholoméus J *Angew. Chem., Int. Ed* 2014, 53, 7300.
- (10). Yang M; Su B; Wang Y; Chen K; Jiang X; Zhang Y-F; Zhang X-S; Chen G; Cheng Y; Cao Z; Guo Q-Y; Wang L; Shi Z-J *Nat Commun* 2014, 5, 4707. [PubMed: 25140832]
- (11). Perry RH; Cahill TJ; Roizen JL; Du Bois J; Zare RN *Proc. Natl. Acad. Sci* 2012, 109, 18295. [PubMed: 23091019]
- (12). (a)Javed MI; Wyman JM; Brewer M *Org. Lett* 2009, 11, 2189. [PubMed: 19371074] (b)Wyman J; Javed MI; Al-Bataineh N; Brewer M *J. Org. Chem* 2010, 75, 8078. [PubMed: 21067195] (c)Al-Bataineh NQ; Brewer M *Tetrahedron Lett* 2012, 53, 5411. (d)Bercovici DA; Brewer M *J. Am. Chem. Soc* 2012, 134, 9890. [PubMed: 22680985] (e)Bercovici DA; Ogilvie JM; Tsvetkov N; Brewer M *Angew. Chem., Int. Ed* 2013, 52, 13338.
- (13). Hong X; Liang Y; Brewer M; Houk KN *Org. Lett* 2014, 16, 4260. [PubMed: 25058856]
- (14). Hong X; Küçük HB; Maji MS; Yang Y-F; Rueping M; Houk KN *J. Am. Chem. Soc* 2014, 136, 13769. [PubMed: 25226575] and references therein.
- (15). Fiori KW; Espino CG; Brodsky BH; Du Bois J *Tetrahedron* 2009, 65, 3042.
- (16). Paradine SM; White MC *J. Am. Chem. Soc* 2012, 134, 2036. [PubMed: 22260649]
- (17). Alderson JM; Phelps AM; Scamp RJ; Dolan NS; Schomaker JM *J. Am. Chem. Soc* 2014, 136, 16720. [PubMed: 25386769]
- (18). Keinan E; Greenspoon N *J. Am. Chem. Soc* 1986, 108, 7314.
- (19). Badiei YM; Dinescu A; Dai X; Palomino RM; Heinemann FW; Cundari TR; Warren TH *Angew. Chem., Int. Ed* 2008, 47, 9961.
- (20). Nägeli I; Baud C; Bernardinelli G; Jacquier Y; Moraon M; Müllet P *Helv. Chim. Acta* 1997, 80, 1087.
- (21). Mueller P; Baud C; Naegeli I *J. Phys. Org. Chem* 1998, 11, 597.
- (22). Frisch MJ; Trucks GW; Schlegel HB; Scuseria GE; Robb MA; Cheeseman JR; Scalmani G; Barone V; Mennucci B; Petersson GA; Nakatsuji H; Caricato M; Li X; Hratchian HP; Izmaylov AF; Bloino J; Zheng G; Sonnenberg JL; Hada M; Ehara M; Toyota K; Fukuda R; Hasegawa J; Ishida M; Nakajima T; Honda Y; Kitao O; Nakai H; Vreven T; Montgomery JA Jr.; Peralta JE; Ogliaro F; Bearpark M; Heyd JJ; Brothers E; Kudin KN; Staroverov VN; Kobayashi R; Normand J; Raghavachari K; Rendell A; Burant JC; Iyengar SS; Tomasi J; Cossi M; Rega N; Millam JM; Klene M; Knox JE; Cross JB; Bakken V; Adamo C; Jaramillo J; Gomperts R; Stratmann RE; Yazyev O; Austin AJ; Cammi R; Pomelli C; Ochterski JW; Martin RL; Morokuma K; Zakrzewski VG; Voth GA; Salvador P; Dannenberg JJ; Dapprich S; Daniels AD; Farkas O;

Foresman JB; Ortiz JV; Cioslowski J; Fox DJ *Gaussian 09*, revision D.01; Gaussian, Inc.: Wallingford, CT, 2009.

- (23). (a)Zhao Y; Truhlar D *Theor. Chem. Acc* 2008, 120, 215.(b)Zhao Y; Truhlar DG *Acc. Chem. Res* 2008, 41, 157. [PubMed: 18186612]
- (24). Marenich AV; Cramer CJ; Truhlar DG *J. Phys. Chem. B* 2009, 113, 6378. [PubMed: 19366259]
- (25). Singleton DA; Hang C; Szymanski MJ; Greenwald EE *J. Am. Chem. Soc* 2003, 125, 1176. [PubMed: 12553813]
- (26). The criteria to terminate trajectories were: C20-N3<1.60 and H21-N3<1.10, or C20-H21<1.10 and C20-N3>5.00 (The atom index is shown in Figure 3). If none of the above criteria were met, a trajectory was terminated after 500 fs. About 10% of trajectories recross the transition state region to form the same species in the forward and reverse directions, and these trajectories are not discussed.
- (27). The possible singlet diradical transition state cannot be located, all optimizations for the corresponding singlet diradical intermediate led to the stable close-shell species 10. The energy of the singlet species based on the optimized structure of triplet 13 is 29.2 kcal/mol less stable than 10.
- (28). (a)Newcomb M; Toy PH *Acc. Chem. Res*, 2000, 33, 449. [PubMed: 10913233] (b)Groves JTJ *Inorg. Biochem* 2006, 100, 434.
- (29). Zou L; Paton RS; Eschenmoser A; Newhouse TR; Baran PS; Houk KN *J. Org. Chem* 2013, 78, 4037. [PubMed: 23461537]
- (30). The calculated chemoselectivity of substrate **1j** is different than the experimental value (Scheme 6) because the tertiary C-H amination transition state is over-stabilized by the solvation energy corrections. In gas phase calculations, benzylic C-H amination is favored by 2.6 kcal/mol. With the CPCM model (Radii=UA0), the chemoselectivity is 1.4 kcal/mol in favor of tertiary C-H amination.
- (31). When n = 3, the electrophilic aromatic substitution appears to be attainable. However, neither reaction occurred experimentally and the only identifiable product of this reaction was the corresponding ketone, which presumably forms by hydrolysis during workup.

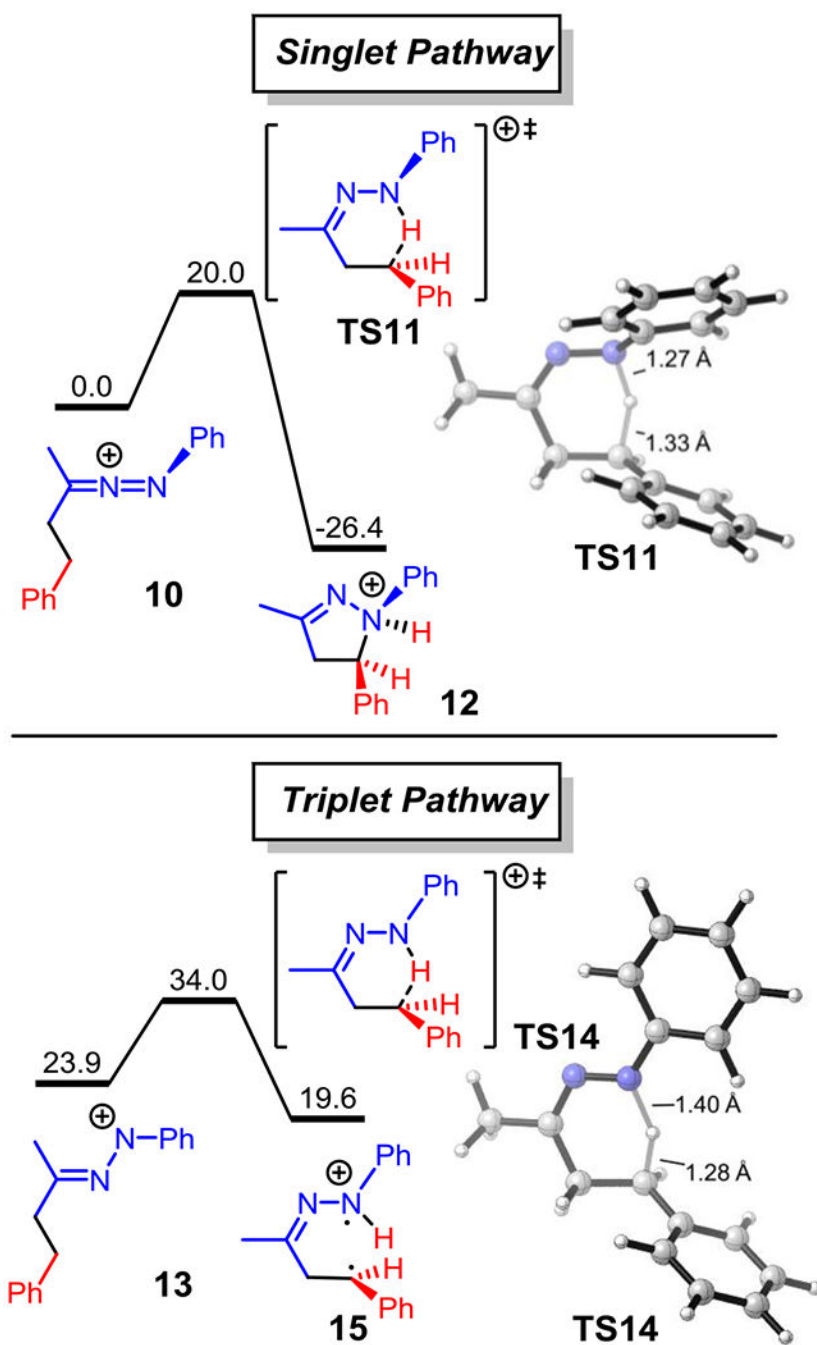


**Figure 1.** The optimized structures of transition states and free energy changes of singlet and triplet C-H amination pathways of aryl-1-aza-2-azoniallene **10**. Gibbs free energies are in kcal/mol.

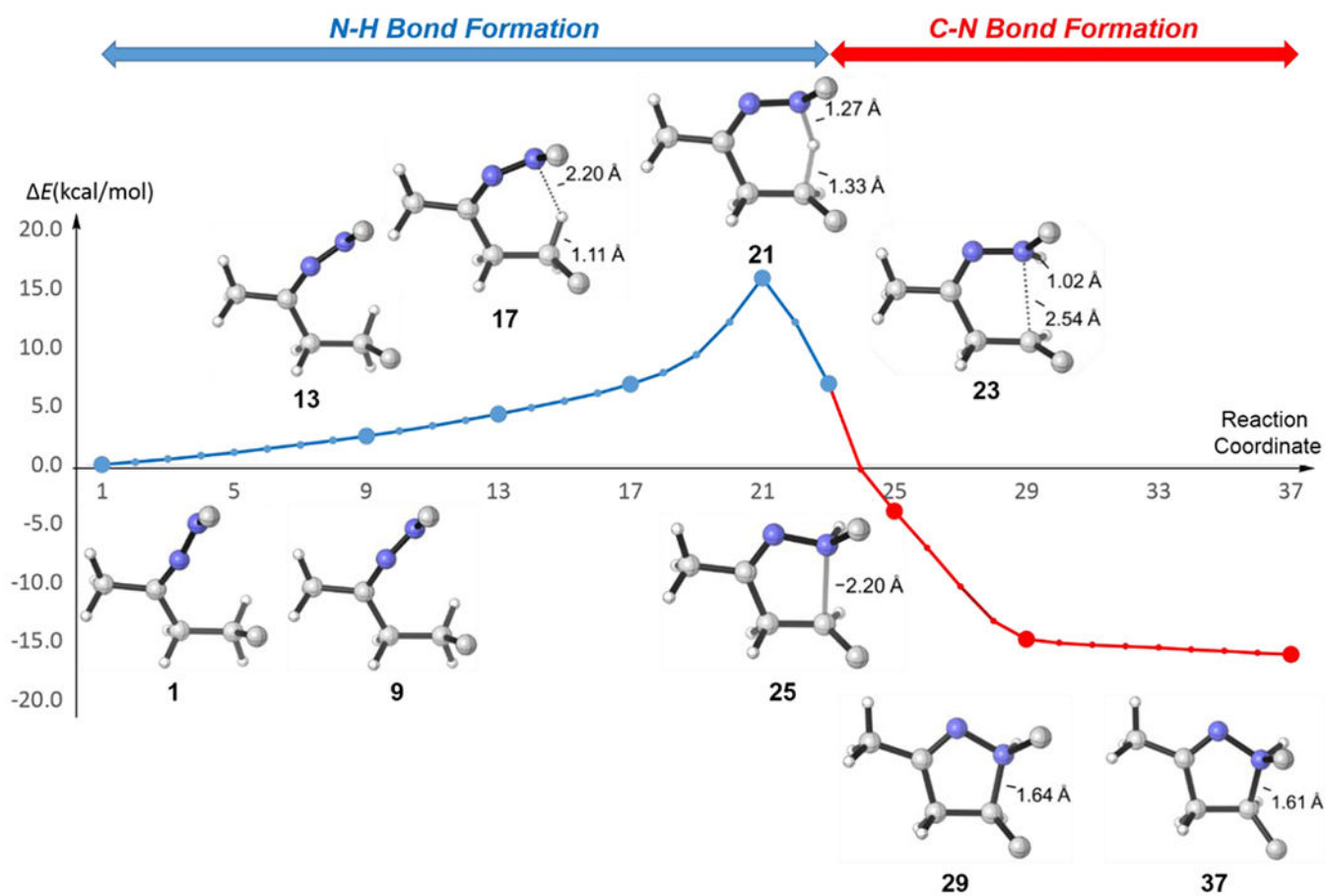


**Figure 2.** The IRC of transition state **TS11**, only the  $\alpha$ -carbons of the phenyl groups are shown for simplicity, and the boundary between N-H and C-N bond formations is chosen based on the N-H bond distance.

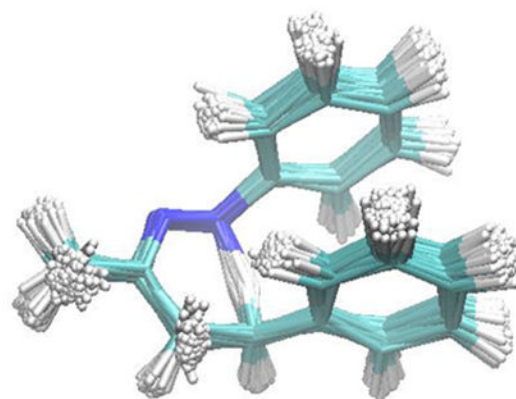
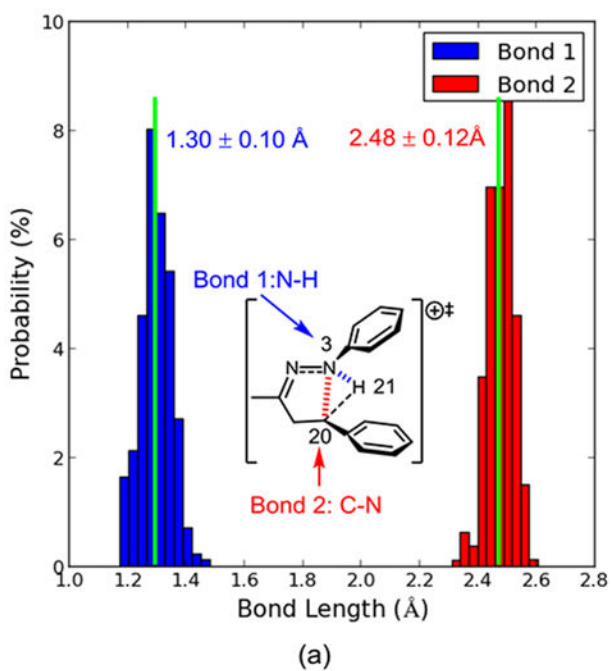


**Figure 3.** (a) The distribution of N-H and C-N bonding lengths in the transition state region of singlet C-H amination pathway at 298K. (b) Superposition of the 256 sampled transition state geometries.

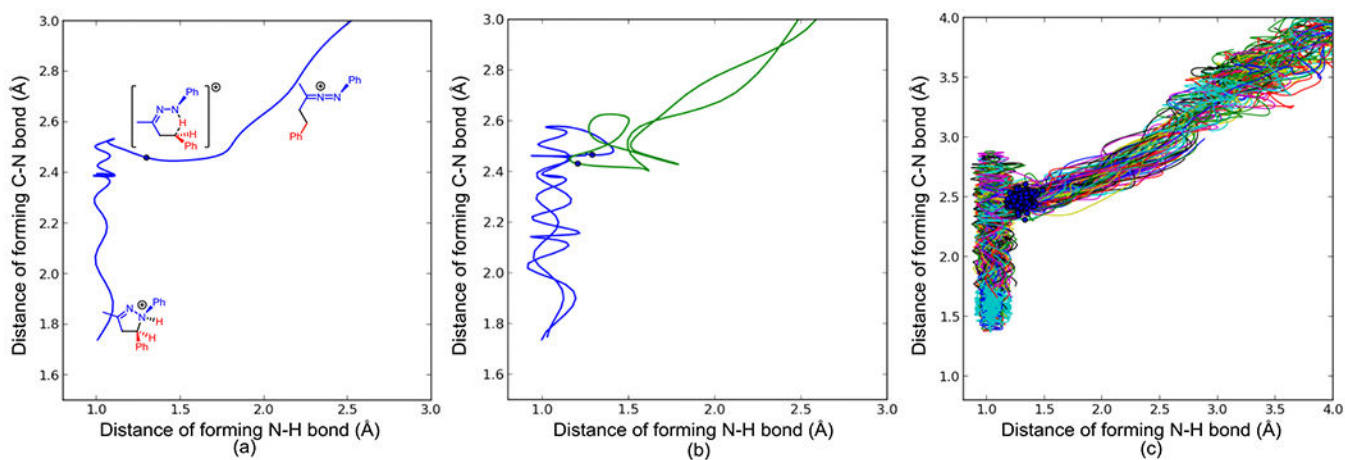


**Figure 4.** Quasi-classical molecular dynamics trajectories for the singlet C-H amination of aryl-1-aza-2-azoniaallene **10**: (a) A productive trajectory. The duration of the trajectory is 110 fs. (b) Two unproductive trajectories. The green trajectory recrosses at reactant side, and the blue trajectory recrosses at the product side. (c) Overlay of 256 trajectories at 298 K.

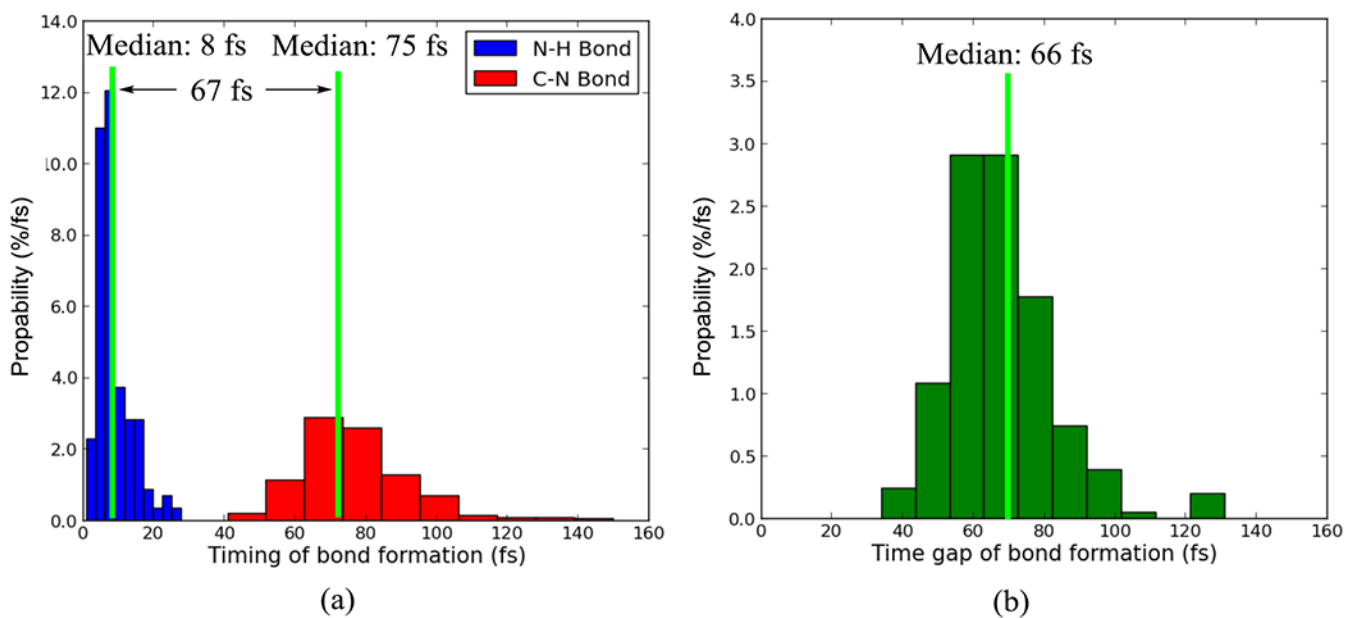
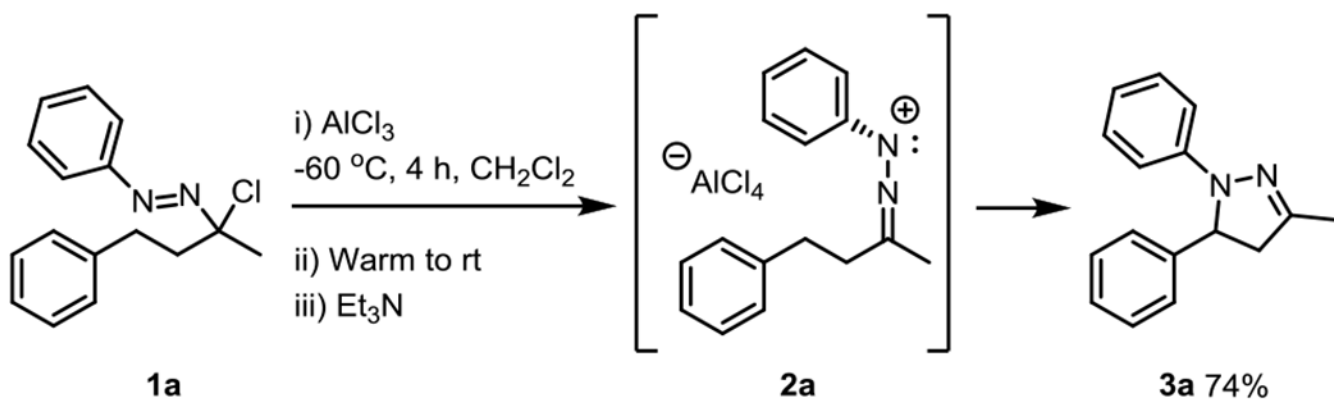
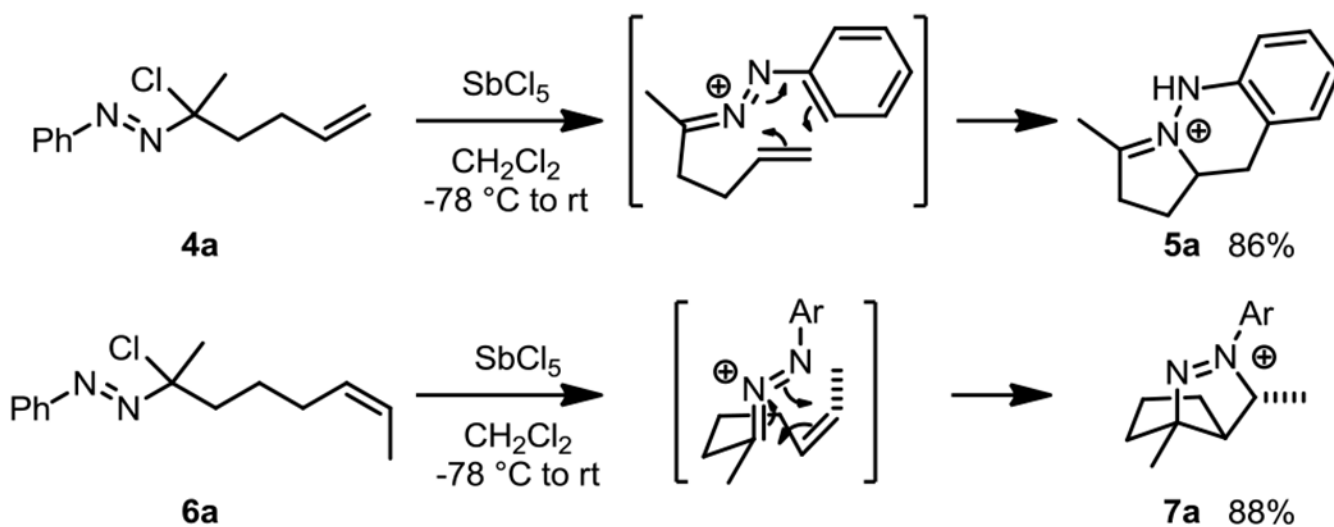


**Figure 5.**  
(a) The distribution of timing of C-N and N-H bond formations at 298K. The starting point (time zero) is each sampled transition state geometry. (b) The distribution of time gap between C-N and N-H bond formations.

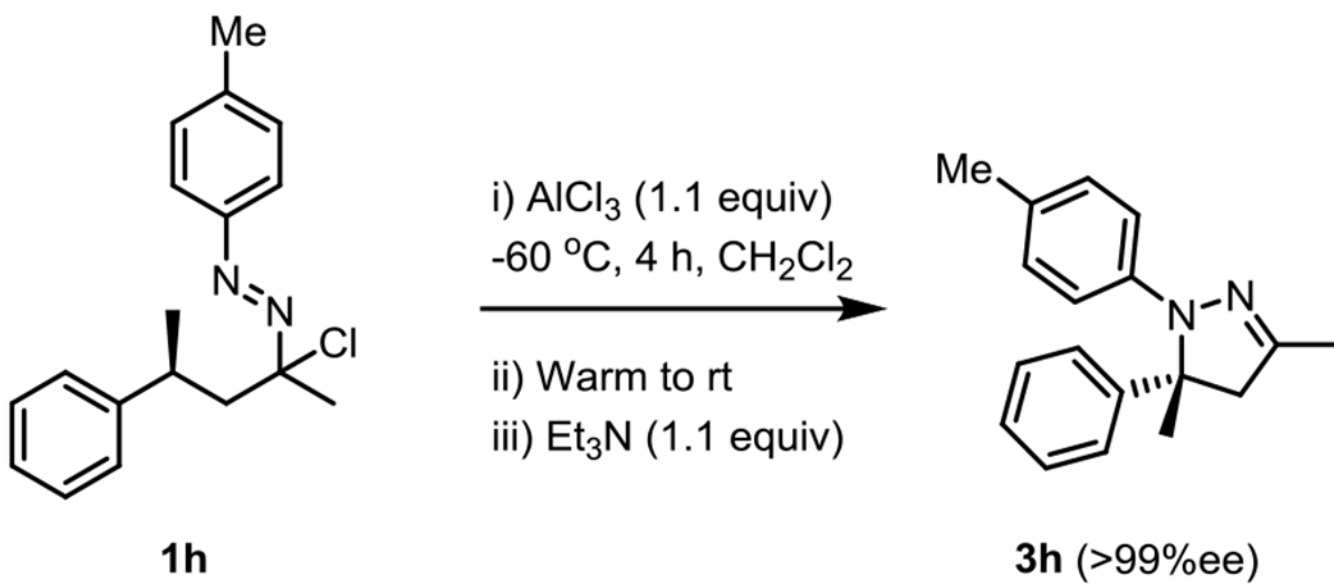


**Scheme 1.**  
Intramolecular benzylic C-H insertion of 1-aza-2-azoniaallene

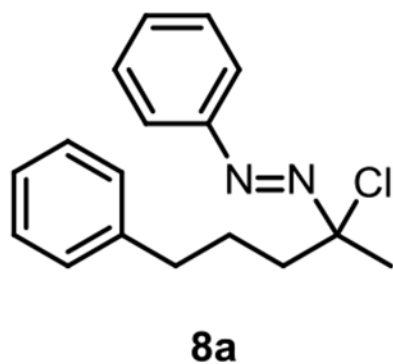




**Scheme 2.**  
Intramolecular cycloadditions of 1-aza-2-azoniaallenes

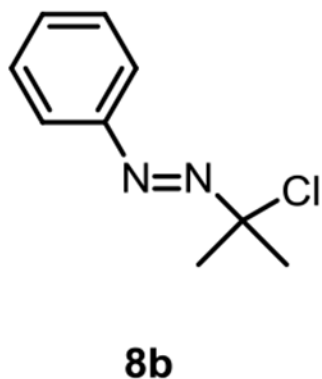
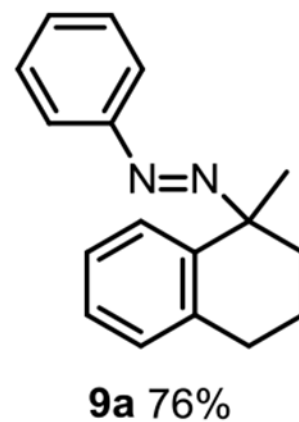


**Scheme 3.**  
Stereospecific C-H insertion at a tertiary benzylic position of 1-aza-2-azoniaallene



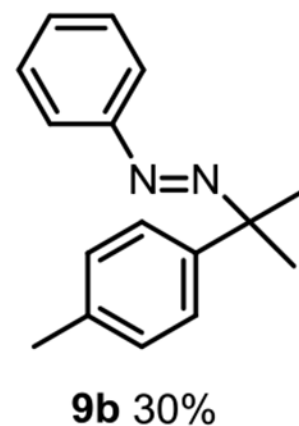
i)  $\text{AlCl}_3$  (1.1 equiv)  
-60 °C, 2 h,  $\text{CH}_2\text{Cl}_2$

ii) Warm to rt  
iii)  $\text{Et}_3\text{N}$  (1.1 equiv)



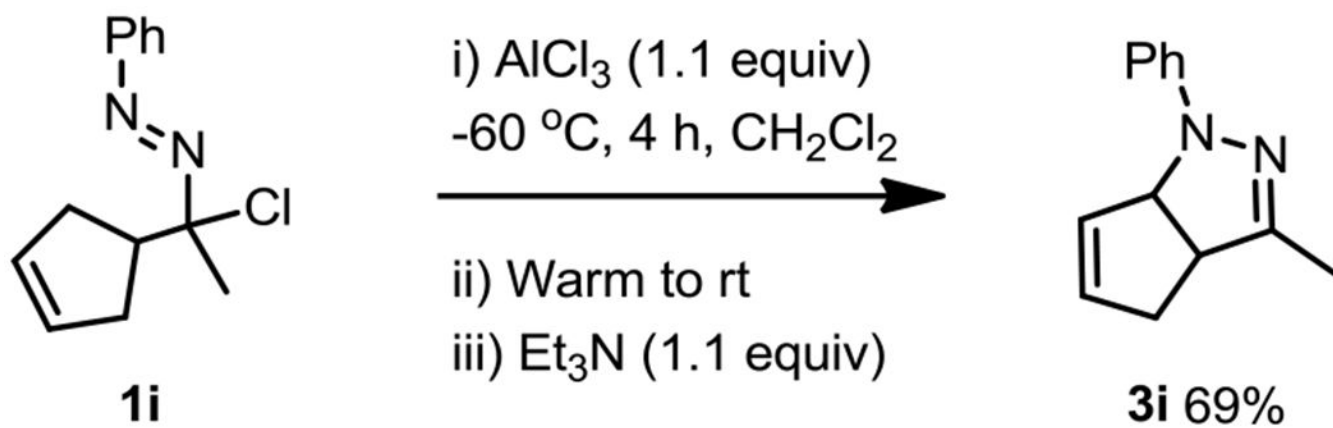
i)  $\text{AlCl}_3$  (1.1 equiv)  
-78 °C, 1 h,  $\text{CH}_3\text{Ph}$

ii) Warm to 0 °C  
iii)  $\text{Et}_3\text{N}$  (1.1 equiv)

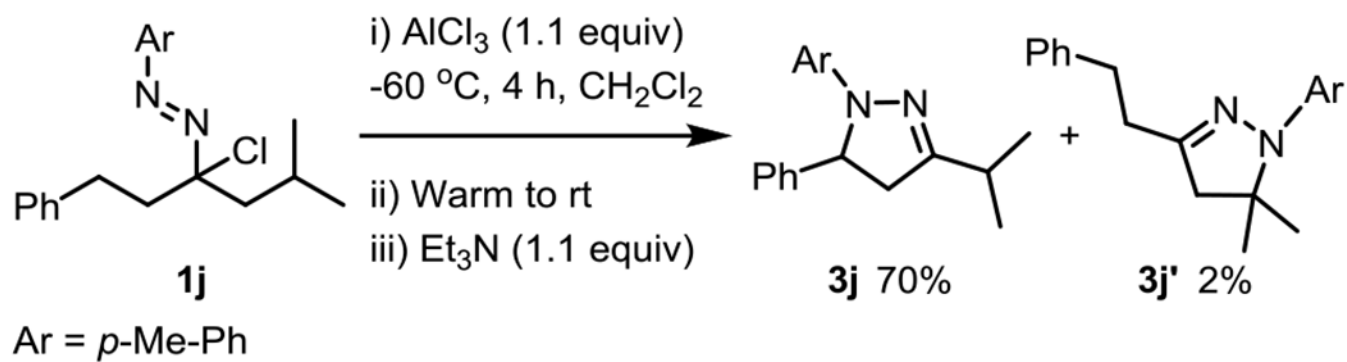


**Scheme 4.**

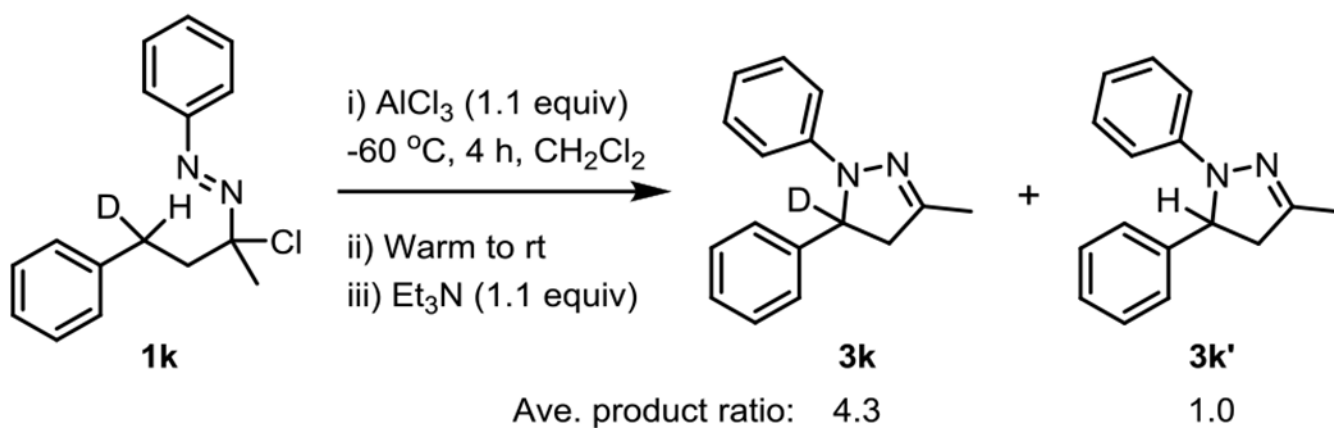
Effect of tether length on intramolecular reactions of 1-aza-2-azoniaallenes



**Scheme 5.**  
Intramolecular C-H insertion at allylic position of 1-aza-2-azoniaallene

**Scheme 6.**

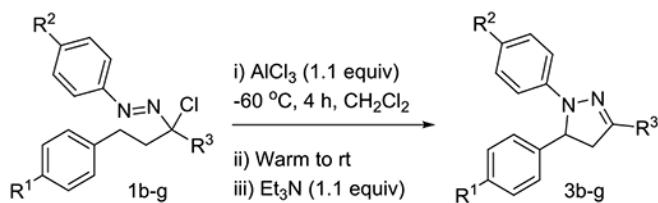
Competition between intramolecular C-H insertions at benzylic and tertiary aliphatic position of 1-aza-2-azoniaallene



**Scheme 7.**  
Experimental kinetic isotope effect

**Table 1.**

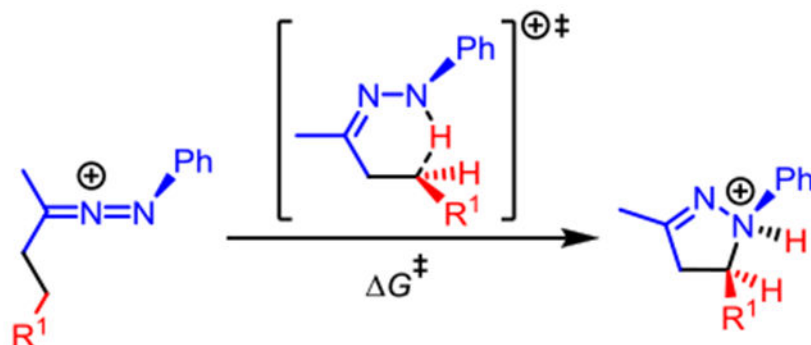
Intramolecular C-H insertions of 1-aza-2-azoniaallenes with electron-rich and electron-poor N-aryl substitutes






| Entry | $\alpha$ -chloroazo | $R^1$          | $R^2$         | $R^3$                                       | Yield |
|-------|---------------------|----------------|---------------|---|-------|
| 1     | 1b                  | H              | Cl            | $\text{CH}_3$                               | 61%   |
| 2     | 1c                  | H              | $\text{CH}_3$ | $\text{CH}_3$                               | 79%   |
| 3     | 1d                  | $\text{OCH}_3$ | Cl            | $\text{CH}_3$                               | 79%   |
| 4     | 1e                  | $\text{CH}_3$  | Cl            | $\text{CH}_3$                               | 65%   |
| 5     | 1f                  | $\text{NO}_2$  | Cl            | $\text{CH}_3$                               | 65%   |
| 6     | 1g                  | $\text{OCH}_3$ | $\text{CH}_3$ | $-(\text{CH}_2)_2-(4\text{-NO}_2)\text{Ph}$ | 92%   |

Table 2.

C-H amination barriers of substituted aryl-1-aza-2-azoniallene cations (Gibbs free energies are in kcal/mol)

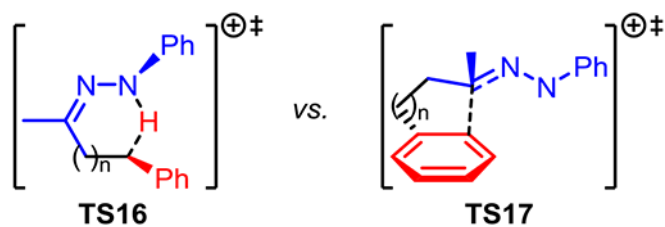


| entry | R <sup>1</sup>  | ΔG <sup>‡</sup> | entry | R <sup>1</sup>   | ΔG <sup>‡</sup> |
|-------|-----------------|-----------------|-------|--|-----------------|
| 1     | Ph              | 20.0            | 12    | OH   | 15.6            |
| 2     | H               | 31.4            | 13    | NH <sub>2</sub>  | 11.7            |
| 3     | Me              | 21.2            | 14    |   | 20.4            |
| 4     | Et              | 21.7            | 15    |  | 25.6            |
| 5     | <i>i</i> Pr     | 22.8            | 16    |  | 16.3            |
| 6     | <i>t</i> Bu     | 22.9            | 17    | <i>o</i> -NO <sub>2</sub> -Ph  | 24.0            |
| 7     | F               | 27.2            | 18    | <i>m</i> -NO <sub>2</sub> -Ph  | 21.3            |
| 8     | Cl              | 29.4            | 19    | <i>p</i> -NO <sub>2</sub> -Ph  | 22.6            |
| 9     | CN              | 33.9            | 20    | <i>o</i> -OMe-Ph   | 19.2            |
| 10    | CF <sub>3</sub> | 38.6            | 21    | <i>m</i> -OMe-Ph   | 19.8            |
| 11    | NO <sub>2</sub> | 35.3            | 22    | <i>p</i> -OMe-Ph   | 17.9            |



**Table 3.**

The Gibbs free energy barriers of C-H amination and electrophilic aromatic substitution of aryl 1-aza-2-azoniallene cations with different tethers (Gibbs free energies are in kcal/mol)



| n              | TS16 | TS17 |
|----------------|------|------|
| 1              | 20.0 | 21.3 |
| 2              | 23.8 | 14.2 |
| 3              | 32.5 | 20.1 |
| intermolecular | 34.4 | 26.5 |